GEOCHRONOMETRIA 48 (2021): 232–241
DOI 10.1515/geochr-2015-0113

Available online at
https://content.sciendo.com/view/journals/geochr/geochr-overview.xml

Conference Proceedings of the 5th Asia Pacific Luminescence and Electron Spin Resonance Dating Conference Oct 15th-17th, 2018, Beijing, China

Guest Editor: Grzegorz Adamiec

HIGH RESOLUTION QUARTZ OSL AND K-FELDSPAR post-IR IRSL DATING OF LOESS IN THE CENTRAL SHANDONG MOUNTAINS (EASTERN CHINA)

QIUYUE ZHAO[1], MIN DING[1], SHUZHEN PENG[1], LUO WANG[2], WEI ZHANG[1], BO SONG[3], RUI ZHOU[4], JUNSHENG YUE[1] and DONGDONG ZHENG[1]

[1]*Key Laboratory of Tourism and Resources Environment in Universities of Shandong, Taishan University, 271000 Taian, China*
[2]*Key Laboratory of Cenozoic Geology and Environment, Institute of Geology and Geophysics, Chinese Academy of Sciences, Beijing 100029, China*
[3]*Beijing Jing Yuan School, 100040 Beijing, China*
[4]*Institute of Earthquake Forecasting, China Earthquake Administration, 100036 Beijing, China*

Received 15 January 2019 Accepted 12 July 2019

Abstract: The loess sediments widely distributed in the Central Shandong Mountains are sensitive records of East Asian monsoon changes for situating in a key region connected to the Eurasian Plate and the Pacific Ocean. However, the detailed processes of palaeoclimatic changes are poorly understood for the lack of high-resolution chronology. In this study, the chronology of Heishan loess palaeosol sequence in the Central Shandong Mountains is investigated using quartz SAR OSL and K-feldspar post-IR infrared (IR) stimulated luminescence (post-IR IRSL) dating method. The quartz is sensitive, fast component dominated and saturate at ~150 Gy (~50 ka). The measured K-feldspar $pIRIR_{290}$ D_e showed no dependency on the first IR stimulation temperature between 50°C and 260°C. The K-feldspar $pIRIR_{290}$ ages are consistent with the stratigraphy up to ~75 ka. In establishing the chronological sequence for the study section, quartz OSL ages <50 ka and the K-feldspar $pIRIR_{290}$ ages >50 ka were selected. Derived sedimentation rates show two relatively rapid stages of ~32.0 ± 5.5 cm/ka for the palaeosol (~11–8 ka) and ~54.8 ± 1.1 cm/ka for the loess (~34–30 ka). An erosional hiatus of loess between ~30 ka and ~17 ka is identified. We conclude that the $pIRIR_{290}$ of loess sediments is applicable for samples during ~8–75 ka.

Keywords: quartz SAR OSL, K-feldspar post-IR IRSL, last glacial period, hiatus, loess-palaeosol sequence.

Corresponding authors: S. Peng; Q. Zhao
e-mails: shuzhenpeng@sohu.com; cnuqyzhao@sina.com

ISSN 1897-1695 (online), 1733-8387 (print)

1. INTRODUCTION

The loess of the Chinese Loess Plateau (CLP) potentially provide an important source of information about history of continental aridity, uplift of the Tibetan Plateau, global atmospheric circulation and are closely related to the evolution of the polar ice sheets (e.g. Pye, 1995; Ding *et al.*, 1999; An *et al.*, 2001; Guo *et al.*, 2002; Lu *et al.*, 2004; Song *et al.*, 2007; Hao *et al.*, 2012). In China, loess sediments not only deposit on the Loess Plateau but also accumulate in other arid, semi-arid and semi-humid areas. In recent years, increasing interest has been focused on the loess outside the CLP in order to derive more local to global palaeoenvironmental information from a wider area (e.g. Fang *et al.*, 1999; Hao *et al.*, 2010; Lai *et al.*, 2001; Yang *et al.*, 2014; Yi *et al.*, 2017).

To the east of the CLP, loess sediments widely distributed in Central Shandong Mountains (CSM) are significant terrestrial palaeoclimatic archives in the semi-humid region of eastern China. It is also sensitive records of East Asian monsoon changes for situating in a key region connected to the Eurasian Plate and the Pacific Ocean. However, compared with the detailed work on the loess sediments from the CLP, loess sediments in CSM region have not been well investigated. In recent years, the relatively unified understanding of the loess sedimentation on CSM mainly focused on its genesis and provenance: (1) the loess of CSM was characterized by typical aeolian based on the field stratigraphic characteristics and grain size analysis (Liu *et al.*, 2000; Zhang *et al.*, 2004; Peng *et al.*, 2007); (2) the provenance of loess in the CSM region are relatively stable based on systematic sedimentology, geochemistry and mineralogy studies (Zhang *et al.*, 2005; Peng *et al.*, 2007, 2016; Xu *et al.*, 2015, 2017). However, research into the stratigraphy and palaeoclimatology in the CSM region are limited due to the controversy of chronology. Zheng *et al.* (1994) obtained the boundary Thermoluminescence (TL) ages between the last interglacial palaeosol and last glacial loess at Zibo section is 143 ± 11 ka. Peng *et al.* (2011) put forward that the quartz optically stimulated luminescence (OSL) age of the bottom of the last glacial loess at Qingzhou section is 74.8 ± 4.6 ka. While the latter chronology seems to be more reasonable on the basis of the correlation with established loess-palaeosol sequences in the CLP and marine isotope records, there is a lack of robust justification at other loess sections in the CSM region. In addition, a detailed numerical chronology for this region is still rare and younger than ~39 ka (Xu *et al.*, 2014). Long-term reconstruction of climatic changes in CSM is scarce (Peng *et al.*, 2011; Zheng *et al.*, 1994), mainly due to the lack of an accurate and high-resolution chronology for long-term loess-palaeosol sequences.

Rapid developments in OSL dating have proved to be very successful for the signal of dating loess bleached by sunlight before sedimentation (e.g. Buylaert *et al.*, 2008; Lai, 2010; Yi *et al.*, 2016; Stevens *et al.*, 2018). While the quartz OSL signal saturated at relatively low doses (~150 Gy) corresponding upper age limit at ~50 ka using a dose rate of 3–4 Gy/ka (e.g. Chapot *et al.*, 2012, Wang *et al.*, 2018) prevents its use for dating older samples (Wintle and Murry, 2006). The infrared stimulation luminescence (IRSL) signal from feldspar has a much higher saturated dose compared to the quartz signal. However, IRSL tends to age underestimation due to anomalous fading (Wintle, 1973). In order to effectively decrease the anomalous fading impact of feldspar, the stable IRSL signal have been isolated from a higher temperature infrared stimulation signal measured after a lower temperature infrared stimulation (Post-IR IRSL protocols) (Thomsen *et al.*, 2008; Buylaert *et al.*, 2009, 2012; Thiel *et al.*, 2011; Li and Li, 2011, 2012). The improvement of post-IR IRSL protocols have indicated that pIRIR can be successfully utilized to date both younger (<10 ka, e.g. Fu and Li, 2013) and older (>75 ka e.g. Buylaert *et al.*, 2012; Li and Li, 2011, 2012; Chen *et al.*, 2015) samples of loess sediments, providing a basis that the K-feldspar pIRIR dating protocol can compensate the limits of quartz SAR-OSL and has the potential to establish chronologies on loess-palaeosol sequences in this semi-humid zone.

In this study, 20 samples were taken from a 7.5 m loess-palaeosol sequence in CSM region. The objective of this study is two-fold; first, to establish a firm and high-resolution chronology of HS loess using quartz OSL and K-feldspar post-IR IRSL dating over the last interglacial period, which provides a relatively detailed and long-term chronological basis for palaeoenvironmental researches in the study region. The second aim is to investigate the potential of the $pIRIR_{200}IR_{290}$ protocol in CSM loess dating during 10–75 ka. The quartz OSL and feldspar $pIR_{200}IR_{290}$ ages are compared with the loess-palaeosol stratigraphy to determine the applicability of the method for the loess sediments in this semi-humid region.

2. SITE DESCRIPTION AND SAMPLING

CSM region is located in the lower reaches of the Yellow River (**Fig. 1a**, **1b**). The geomorphology of the CSM region is characterized by a serious of low mountains and hills (Mao, 1993), with elevations ranging from 200 to 1545 m above sea level (Peng *et al.*, 2016). The region has a warm and semi-humid monsoon climate, which is characterized by obvious seasonal changes in temperature, precipitation and wind direction. The mean annual temperature is 12.6–14.5°C and the mean annual precipitation vary between 550 mm and 950 mm, but most rainfall (60~70%) occurs in summer from June to August. In winter, the climate is controlled by the Siberia High, and the prevailing wind is northwesterly, and southeasterly winds in summer.

The new Heishan (HS) loess section (36°10.05'N, 116°20.63'E) sampled from the south bank of lower reaches of Yellow River is in the southwest of CSM (**Fig. 1b**).

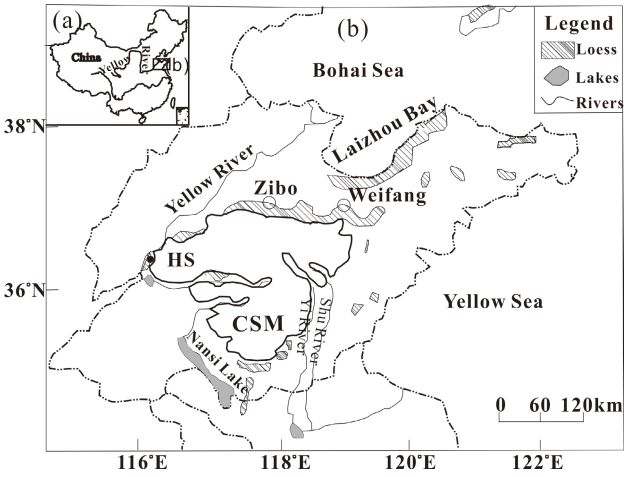

Fig. 1. *(a) Location of the study region of the Central Shandong Mountains. (b) Location of the sampled loess section (HS) in the Central Shandong Mountains.*

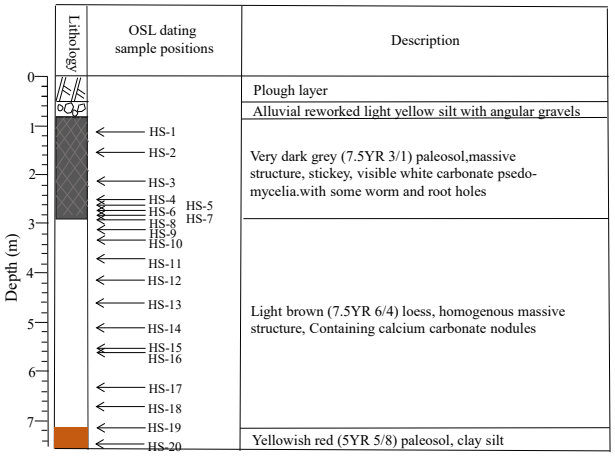

Fig. 2. *The lithology of the studied loess section and the positions of luminescence dating samples.*

The section has a thickness of 7.5 m, with yellow plough horizon (0–1.0 m), greyish black Holocene soil (1.0–2.9 m), Malan loess (2.9–7.1 m) and the last interglacial palaeosol (7.1–7.5 m). Detailed lithological characteristics of each unit are shown in **Fig. 2**.

Twenty samples were collected using light-tight steel tubes (diameter 5 cm, length 20 cm) from a freshly prepared vertical section. The tubes were fully filled with sediments to prevent mixing during transportation. The tubes were then wrapped with aluminium foil at both ends to prevent light exposure and moisture loss for OSL measurement.

3. METHODS

Luminescence sample preparation

Samples were opened under subdued red light conditions, and the outer 3–4 cm layers at the ends of each tube were removed for water content and dose rate analysis. The remaining material at the middle part of the tube was then pretreated using the standard procedures, including treatment with 10% hydrochloric acid (HCl) and 10% hydrogen peroxide (H_2O_2) to remove carbonates and organic matter, respectively. After wet sieving, grains in the range of 63–90 μm were extracted. This coarse fraction was treated with 10% hydrofluoric acid (HF) for 20 min, to remove coatings and the outer alpha-irradiated layer, and then rinsed in 10% HCl for 20 min to remove precipitated fluorides. Subsequently, the remaining grains were separated by heavy liquid to extract quartz grains ($2.58 < \rho < 2.70$ g/cm^{-3}) and K-feldspar grains ($\rho < 2.58$ g/cm^{-3}). Quartz extracts were etched in 40% HF for 1 h and rinsed for 1h in 10% HCl. The purity of quartz was checked by IR depletion ratio method (Duller, 2003) and 110°C TL peak (Li *et al.*, 2002).

Experimental details and protocols

Quartz and K-feldspar measurements were performed on a Risø TL/OSL-DA-20 reader (Bøtter-Jensen *et al.*, 2010) equipped with blue LEDs (470 nm, ~80 mW cm^{-2}) and infrared LEDs (875 nm,~135 mW cm^{-2}) for stimulation in the luminescence dating laboratory of Taishan University. Quartz OSL signals were detected through a 7.5 mm Hoya U-340 glass filter, and K-feldspar post-IR IRSL signals were detected through a combination of Corning 7–59 and Schott BG-39 glass filters, respectively. The ^{90}Sr/^{90}Y beta source was calibrated for both discs and cups by 180–250 μm calibration quartz samples (Hansen *et al.*, 2015). Quartz and K-feldspar grains were mounted on stainless steel discs (5 mm) and cups (3 mm) respectively using silicone oil as adhesive. The stimulation power was set at 90% of the maximum value, and the heating rate is 5°C/s in all thermal treatment.

For quartz OSL, a standard single-aliquot regenerative dose (SAR) protocol (Murray and Wintle, 2000, 2003) was applied for luminescence measurements. The thermal treatment was set as preheat at 260°C and cut-heat at 220°C with blue stimulation at 125°C. The measurement of preheat temperature is described in Section 4. The single aliquot quartz OSL signals were derived from the summation of the initial 0.64 s of stimulation, less an early background of the following 0.64 s of stimulation to minimize a contribution from medium and slow components (Ballarini *et al.*, 2007; Cunningham and Wallinga, 2010). Only D_e estimates with a relative uncertainty of the natural test dose signal less than 10% were accepted. In addition, dose estimates were accepted only if (i) the OSL IR depletion and recycling ratios lay between 0.9 and 1.1 and (ii) sensitivity corrected recuperation signals were consistent with zero at 2σ (Murray and Wintle, 2000, 2003; Wintle and Murray, 2006). These criteria led to the rejection of ~4% of the measured aliquots because

the sensitivity corrected natural signal was in or above saturation of the laboratory dose-response curve.

For K-feldspar, the SAR $pIRIR_{290}$ protocol (Thiel *et al.*, 2011; Buylaert *et al.*, 2012; Li and Li, 2012) was applied to measure the D_e. Samples were stimulated by infrared light at 290°C after stimulation at 200°C. Feldspar (post-IR) IRSL signals were derived from the integral of the first 2 s of post-IR IRSL stimulation, less a background based on the last 50 s.

Dose rate determination

The environmental dose rate was determined from the U and Th concentrations and K contents, measured by neutron activation analysis (NAA) method in the Chinese Atomic Energy Institute. Calculation of the cosmic ray contribution was assessed according to Prescott and Hutton (1994). Measured water content from the HS section varied between 10% and 17%. Based on the water content from previous CSM loess researches (Peng *et al.*, 2011; Kong *et al.*, 2017) and the measured in the lab, water content of 15 ± 5% was used in all dose rate calculations. For quartz, an internal dose rate of 0.06 ± 0.03 Gy/ka was assumed after Mejdahl (1987). For the K-feldspar dose rate, a K concentration of 12.5 ± 0.5% and Rb content of 400 ± 100 ppm was assumed (Huntley and Baril, 1997). A summary of the uranium, thorium and potassium concentrations and the resulting dose rates of quartz and K-feldspar grains are given in **Table 1**.

4. RESULTS AND DISCUSSION

Quartz luminescence characteristics and resulting ages

To select appropriate preheat temperatures for quartz D_e determination, preheat temperature plateau tests were used to assess the D_e dependence on preheat temperature for representative samples HS-4 and HS-16 (**Fig. 3b**). Preheat temperatures varied between 200°C and 300°C in increments of 20°C were tested. These results suggest that a 260°C preheat and 220°C cut-heat was suitable for quartz D_e determination. The suitability of SAR procedures for D_e determination was further checked by two dose-recovery tests. The dose recovery ratios are 1.01 ± 0.01 (given dose = 36 Gy, n = 10) and 1.01 ± 0.02 (given dose = 120 Gy, n = 9), respectively.

Typical dose-response curve and decay curve of quartz are shown in **Fig. 3a**. The blue-light stimulated OSL signals of HS-14 decrease very quickly during the first second of stimulation, indicating that the signal is dominated by the fast component (Jain *et al.*, 2003). The dose-response curves of all the samples were fitted by one single saturating exponential function. The D_e obtained using the SAR protocol for all 20 quartz samples range from 26.9 ± 1.2 Gy to 188.6 ± 26.2 Gy (**Table 1**). The quartz age increases with depth from 8.5 ± 0.4 ka to 66.7 ± 3.9 ka.

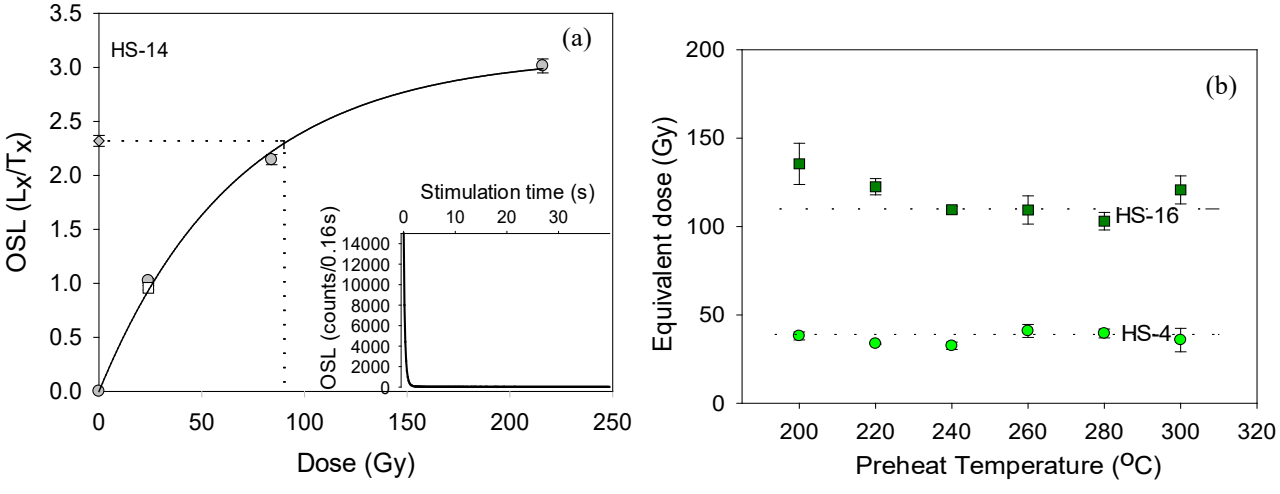

Fig. 3. *Coarse-grain quartz luminescence characteristics. (a) Representative small aliquot dose-response curve (preheat 260°C for 10 s, cut heat 220°C) for sample HS-14 showing recycling and recuperation (open symbols) and the interpolation of the sensitivity-corrected natural signal onto the dose response curve. Inset shows the natural decay curve. (b) Preheat plateau tests of samples HS-4 and HS-16. Three aliquots were measured at each temperature, and error bars represent one standard error. The dashed line is drawn at the average D_e over the 200–300°C interval.*

Table 1. *Summary of the burial depth, radionuclide concentrations, calculated dose rate, quartz and feldspar D_e values and luminescence ages. The water content is assumed to be 15 ± 5%. A residual dose of 6.2 ± 0.4 Gy was subtracted from the measured feldspar $pIRIR_{290}$ D_e values. (n) represents the number of aliquots contributing to the D_e, 1 represents quartz and 2 is feldspar. Uncertainties represent one standard error.*

Sample Code	Depth (m)	U (ppm)	Th (ppm)	K (%)	Q-dose Rate (Gy ka^{-1})	Feldspar-dose Rate (Gy ka^{-1})	Q-D_e (Gy)	Feldspar-D_e (Gy)	Corrected Feldspar-D_e (Gy)	Aliquots (n)	Q-Age (ka)	Corrected Feldspar-age (Gy)
HS-1	1.1	2.16 ± 0.04	11.80 ± 0.03	2.13 ± 0.03	3.20 ± 0.05	3.65 ± 0.09	26.9 ± 1.2	42.9 ± 1.0	36.7 ± 1.1	$12^1/10^2$	8.5 ± 0.4	10.1 ± 0.3
HS-2	1.5	2.31 ± 0.04	11.60 ± 0.03	2.09 ± 0.03	3.14 ± 0.05	3.62 ± 0.09	24.3 ± 1.2	44.4 ± 1.0	38.2 ± 1.1	$10^1/9^2$	7.8 ± 0.4	10.5 ± 0.4
HS-3	2.1	2.20 ± 0.04	11.00 ± 0.03	2.13 ± 0.03	3.10 ± 0.05	3.58 ± 0.09	28.4 ± 0.9	40.0 ± 0.8	33.8 ± 0.9	$10^1/9^2$	9.2 ± 0.3	9.4 ± 0.4
HS-4	2.5	2.42 ± 0.04	12.10 ± 0.03	2.14 ± 0.03	3.22 ± 0.05	3.70 ± 0.09	35.1 ± 1.9	48.0 ± 0.8	41.8 ± 0.9	$15^1/10^2$	10.9 ± 0.6	11.3 ± 0.4
HS-5	2.6	1.96 ± 0.04	11.10 ± 0.03	1.97 ± 0.03	2.91 ± 0.10	3.39 ± 0.13	35.4 ± 0.9	47.1 ± 1.0	40.9 ± 1.1	$13^1/9^2$	12.2 ± 0.6	12.1 ± 0.5
HS-6	2.7	2.04 ± 0.04	11.50 ± 0.03	1.95 ± 0.03	2.93 ± 0.05	3.41 ± 0.09	43.9 ± 1.4	44.2 ± 1.5	38.0 ± 1.6	$12^1/9^2$	15.0 ± 0.6	11.1 ± 0.6
HS-7	2.8	2.17 ± 0.04	12.10 ± 0.03	2.01 ± 0.03	3.10 ± 0.10	3.53 ± 0.13	51.9 ± 1.6	68.3 ± 1.1	62.1 ± 1.1	$12^1/9^2$	17.0 ± 0.8	17.6 ± 0.8
HS-8	2.9	2.40 ± 0.04	12.10 ± 0.03	2.18 ± 0.03	3.24 ± 0.05	3.72 ± 0.09	55.5 ± 2.6	77.1 ± 1.5	70.9 ± 1.6	$12^1/10^2$	17.1 ± 0.9	19.1 ± 0.6
HS-9	3.1	2.07 ± 0.04	12.10 ± 0.03	2.02 ± 0.03	3.03 ± 0.11	3.51 ± 0.13	48.9 ± 1.4	81.4 ± 1.5	75.2 ± 1.5	$12^1/10^2$	16.1 ± 0.8	21.4 ± 0.9
HS-10	3.3	2.01 ± 0.04	11.90 ± 0.03	1.86 ± 0.03	2.86 ± 0.11	3.34 ± 0.13	97.1 ± 4.8	108.1 ± 1.3	101.9 ± 1.4	$12^1/10^2$	33.9 ± 2.1	30.5 ± 1.3
HS-11	3.7	2.31 ± 0.04	12.30 ± 0.03	2.09 ± 0.03	3.18 ± 0.12	3.63 ± 0.09	95.5 ± 5.7	115.7 ± 1.9	109.5 ± 1.9	$10^1/9^2$	30.4 ± 1.9	30.2 ± 0.9
HS-12	4.2	2.45 ± 0.04	11.70 ± 0.03	1.73 ± 0.03	2.82 ± 0.05	3.30 ± 0.09	88.4 ± 2.4	101.1 ± 1.8	94.9 ± 1.8	$10^1/9^2$	31.4 ± 1.0	28.8 ± 0.9
HS-13	4.6	2.44 ± 0.04	11.10 ± 0.03	1.99 ± 0.03	3.00 ± 0.05	3.48 ± 0.09	96.2 ± 1.9	107.7 ± 1.0	101.5 ± 1.1	$10^1/9^2$	32.1 ± 0.8	29.2 ± 0.8
HS-14	5.1	2.95 ± 0.04	11.00 ± 0.03	1.95 ± 0.03	3.06 ± 0.05	3.55 ± 0.09	99.6 ± 2.1	116.8 ± 1.7	110.6 ± 1.7	$15^1/9^2$	32.6 ± 0.9	31.2 ± 0.9
HS-15	5.5	2.54 ± 0.04	12.20 ± 0.03	1.97 ± 0.03	3.06 ± 0.05	3.55 ± 0.09	103.1 ± 2.0	128.4 ± 1.6	122.2 ± 1.6	$12^1/9^2$	33.7 ± 0.9	34.5 ± 1.0
HS-16	5.6	2.32 ± 0.04	11.20 ± 0.03	1.70 ± 0.03	2.72 ± 0.10	3.20 ± 0.12	111.3 ± 3.0	137.1 ± 0.9	130.9 ± 0.9	$16^1/9^2$	41.0 ± 1.9	40.9 ± 1.6
HS-17	6.3	2.21 ± 0.04	8.99 ± 0.03	1.93 ± 0.03	2.75 ± 0.05	3.23 ± 0.08	146.3 ± 6.6	152.3 ± 2.4	146.1 ± 2.5	$12^1/9^2$	53.2 ± 2.6	45.3 ± 1.4
HS-18	6.7	2.17 ± 0.04	10.70 ± 0.03	1.79 ± 0.03	2.72 ± 0.05	3.20 ± 0.08	167.6 ± 5.6	168.0 ± 2.4	161.8 ± 2.4	$12^1/9^2$	61.6 ± 2.3	50.5 ± 1.5
HS-19	7.1	2.22 ± 0.04	10.80 ± 0.03	1.67 ± 0.03	2.63 ± 0.05	3.11 ± 0.08	163.3 ± 9.1	208.7 ± 4.3	202.5 ± 4.3	$10^1/9^2$	62.0 ± 3.6	65.0 ± 2.2
HS-20	7.5	2.23 ± 0.04	11.10 ± 0.03	1.69 ± 0.03	2.67 ± 0.05	3.15 ± 0.08	178.0 ± 9.9	242.9 ± 3.1	236.7 ± 3.1	$12^1/9^2$	66.7 ± 3.9	75.2 ± 2.2

K-feldspar luminescence characteristics and ages

Representative decay curves and dose-response curves for the coarse-grained K-feldspar of sample HS-19 are shown in **Fig. 4a**, **4b**. Based on model predictions, the stability of the post-IR IRSL signal may be dependent on the first IR stimulation temperature or wavelength (Jain and Ankjærgaard, 2011; Li and Li, 2011). Buylaert *et al.* (2012) have suggested the application of a first IR stimulation temperature plateau to investigate signal stability. A series of first stimulation temperatures, ranging from 50°C to 260°C (in increments of 30°C) were applied on samples of HS-3 and HS-20 (**Fig. 4c**), which demonstrates that the D_e is not dependent on the first IR stimulation temperature in a temperature range of 50°C to 260°C (**Fig. 4c**). However, some researches (e.g. Li and Li, 2012; Yi *et al.*, 2016; Stevens *et al.*, 2018) indicate that the first IR stimulation temperature of 200°C prior the second IR stimulation at 290°C ($pIR_{200}IR_{290}$) is more stable than the first IR stimulation temperature of 50°C prior the second IR stimulation at 290°C ($pIR_{50}IR_{290}$). Therefore, all doses were measured by $pIR_{200}IR_{290}$.

To check the stability of the $pIR_{200}IR_{290}$ dating, dose recovery tests were performed. Six aliquots of each sample were bleached for 16 h with a Hönle UVACUBE400 solar simulator before they were given a laboratory β dose close to their natural doses (e.g. Qiu and Zhou, 2015, E *et al.*, 2018). Three aliquots were measured using the $pIR_{200}IR_{290}$ method after given a beta dose. The other three aliquots were measured to determine the residual doses. Different laboratory doses were added to three representative natural samples HS-2, HS-7 and HS-20 (given dose is 40, 90 and 240 Gy), the $pIR_{200}IR_{290}$ dose recovery ratios without subtraction of the residual doses are 1.02 ± 0.09, 1.04 ± 0.04 and 1.14 ± 0.09 with a mean value of 1.06 ± 0.04 (n = 9). With subtraction of the residual doses, the dose recovery ratios are 0.93 ± 0.04,

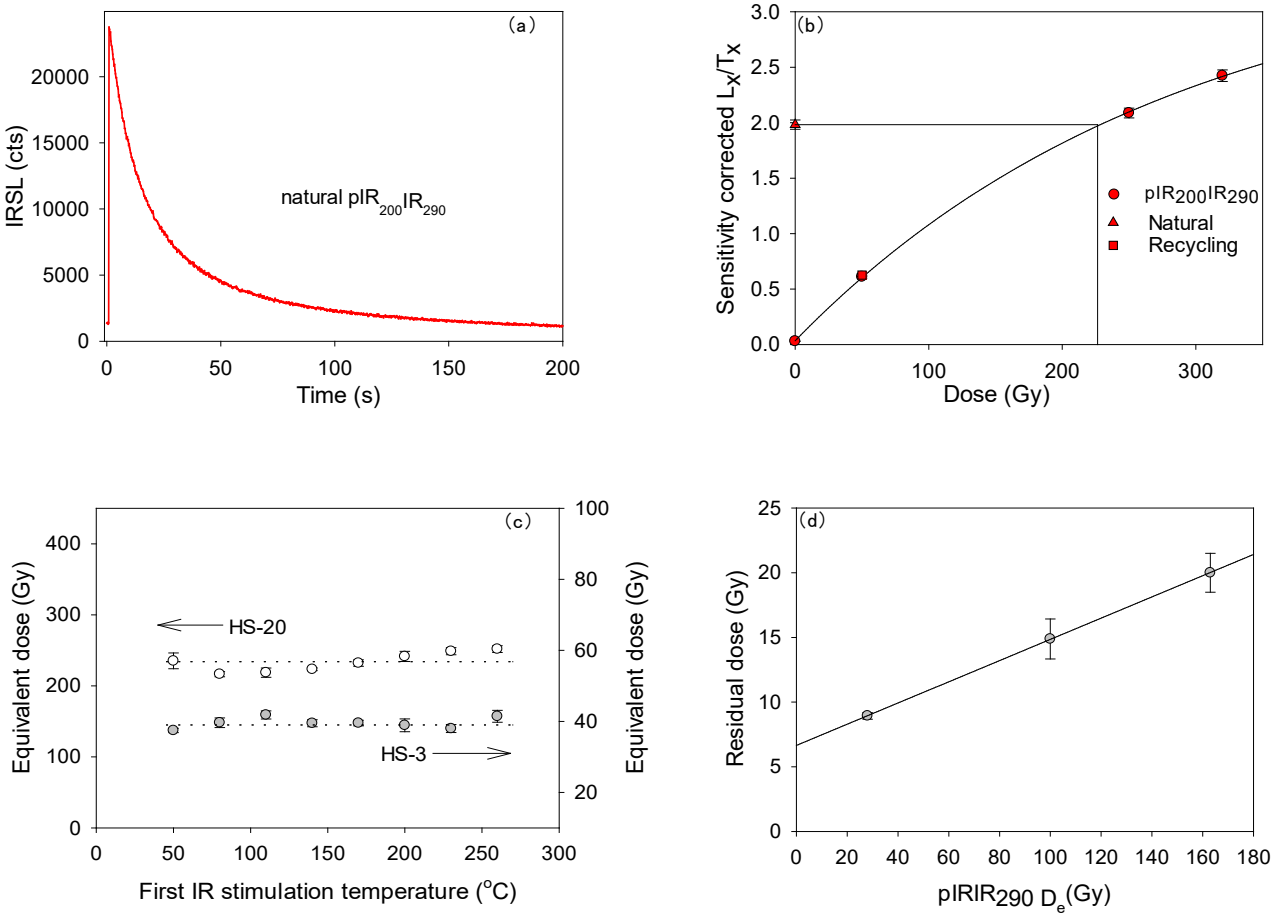

Fig. 4. *Coarse-grain K-feldspar luminescence characteristics. Representative natural decay curve (a) and dose-response curve (b) of $pIR_{200}IR_{290}$ signal for sample HS-19. (c) Dependence of D_e on prior IR stimulation temperatures for the upper (HS-3) and lower sample (HS-20) of the HS section. Three aliquots were measured at each temperature, and error bars represent one standard error. The dash-dot line is drawn at the average D_e over the 50–260°C interval. (d) The pIRIR290 dose residuals after ten days bleach under natural sunlight were plotted against the corresponding equivalent doses.*

1.01 ± 0.03 and 1.11 ± 0.06 with a mean value of 1.02 ± 0.05 (n = 9). It can be seen that the behaviour of $pIR_{200}IR_{290}$ SAR procedure on loess performed well for dose recovery tests.

The post-IR IRSL techniques may overestimate the D_e values due to thermal transfer during high-temperature heat treatment (Buylaert *et al.*, 2012). The residual doses ranging from ~5 Gy to ~60 Gy for the post-IR IRSL signals have been reported from the world under the laboratory and sunlight bleaching conditions (Thomsen *et al.*, 2008; Li and Li, 2011; Thiel *et al.*, 2011; Murray *et al.*, 2014; Yi *et al.*, 2015, 2016). By contrast, much less is known about the residual dose for the loess samples in CSM region. In this study, three coarse loess samples were examined in the experiments. Five aliquots of the samples were bleached under the natural sunlight for ten days, and their residual doses were measured using the $pIR_{200}IR_{290}$ SAR procedure. The results are summarized in **Fig. 4d**. There is a clear tendency for the residual doses to increase with D_e values. Extrapolation of these residual doses to a D_e of zero Gy can be utilized to predict the average residual dose (Buylaert *et al.*, 2012; Yi *et al.*, 2016). The residual dose for the $pIR_{200}IR_{290}$ signal is 6.7 ± 0.4 Gy, which was subtracted from all measured D_e values used to calculate the $pIR_{200}IR_{290}$ ages given in **Table 1**.

The resulting $pIR_{200}IR_{290}$ D_e and ages are summarized in **Table 1**. The D_e values range from 42.9 ± 1.0 Gy for the upper sample to 242.9 ± 3.1 Gy for the lowest sample. The $pIR_{200}IR_{290}$ ages increase with depth from 9.4 ± 0.4 ka to 75.2 ± 2.2 ka (**Table 1**).

Comparison of quartz and feldspar ages

Quartz OSL ages for all samples are plotted against K-feldspar $pIRIR_{290}$ ages in **Fig. 5**. All of the quartz and feldspar ages are consistent with each other in the whole section corresponding to an age of 8~40 ka. The quartz OSL ages ranged from 8.5 ± 0.4 ka for the uppermost sample to 66.7 ± 3.9 ka for the lowest sample are consistently increasing with the depth. The dose of quartz in the 53.2 ± 2.6 ka (HS-17) is 146.3 ± 6.6 Gy, which is almost close to the limits (~150 Gy) of reliable D_e determination using the SAR protocol suggested by Chapot *et al.* (2012). The quartz ages and the saturated dose-response curves suggest that they are already saturation for the samples older than 50 ka. The K-feldspar $pIRIR_{290}$ ages increase systematically from 10.1 ± 0.3 ka to 75.2 ± 2.2 ka and are in stratigraphic order. So the quartz OSL ages <50 ka and the K-feldspar $pIRIR_{290}$ ages >50 ka were selected for establishing the chronological framework for the study profile. Meanwhile, a steep increase of age exists in both chronological sequences at a depth of 3.1 m, indicative of a hiatus in the strata of the loess.

Chronology and sedimentation of the Heishan loess sequence

As demonstrated in **Fig. 6**, the quartz OSL and K-feldspar $pIRIR_{290}$ ages of the HS section indicate that the loess was mainly deposited during the last glaciation and the Holocene. Loess sediments were primarily deposited between ~75 ka and ~30 ka and between 17 ka and ~8 ka, corresponding to MIS 4 to MIS 3 and MIS 1 (Lisiecki and Raymo, 2005), respectively. A hiatus of ~13 ka occurred between ~30 and ~17 ka, generally corresponding to MIS 2 (Lisiecki and Raymo, 2005). We suggest caution when using the loess sediments in this area to obtain the information of palaeoenvironmental changes, especially during the glacial stages such as MIS 2. Lu *et al.* (2006) identified a discontinuity of loess sedimentation between ~15 ka and 10 ka. They implied that wind erosion related to a cold-dry climate during

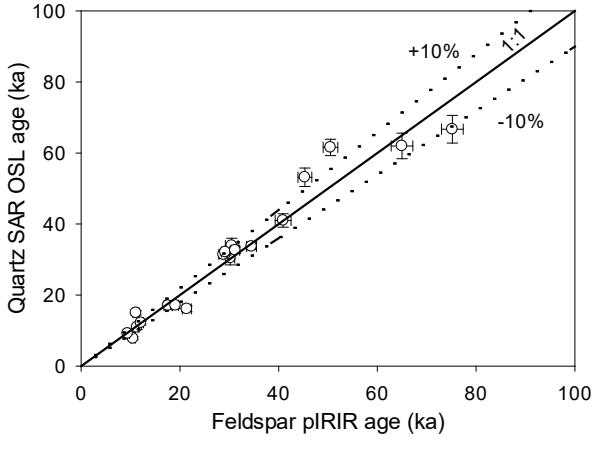

Fig. 5. *Comparison between quartz OSL and K-feldspar $pIR_{200}IR_{290}$ ages.*

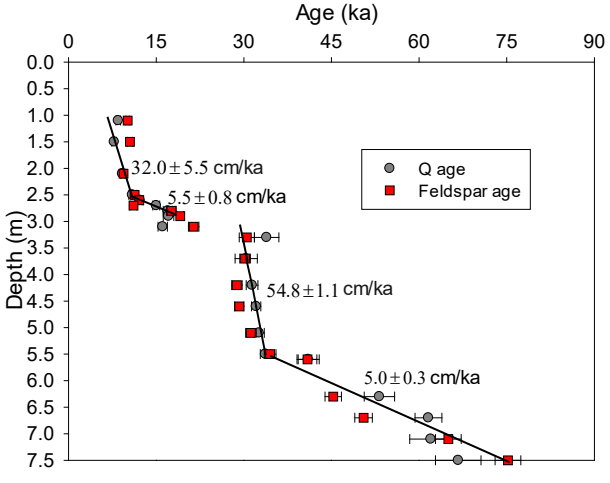

Fig. 6. *Quartz OSL and K-feldspar post-IR IRSL ages of HS loess section.*

MIS 2 might be the primary cause of this hiatus in CLP loess sequences. Buylaert *et al.* (2008) reported that a hiatus was identified from 30 ka to 20 ka (MIS 2) at Tuxiangdao (Xining, western of the CLP) loess section. E *et al.* (2018) also tested a hiatus between 39 ka and 11 ka (MIS 2 and MIS 3) at the Hebei section in the northeast Tibetan Plateau by high-resolution OSL dating, and they attributed it to the deflation at the same time as the CLP is accumulating. Wang *et al.* (2018) also detected a gap in deposition between 25 and 2 ka (MIS 2) at the Ledu loess section in the Huangshui river valley on the northeastern Tibetan Plateau by high-resolution OSL dating, and they attributed it to the erosion events or lower accumulation rate. There seems a sedimentation hiatus in the Mangshan loess during 30–20 ka (MIS 2, Qiu and Zhou, 2015) and Xiashu loess within the period of 30–0 ka (MIS 1 and MIS 2, Yi *et al.*, 2017). It seems that loess closed to desert boundaries, or adjacent to source regions of CLP, or neighbour the major river systems such as the Yangtze River or the Yellow River, often deposited episodically or was eroded during MIS 2.

The dust source of HS loess section in the CSM region might be proximal and most likely from the fluvial deposits (Peng *et al.*, 2016). The dust accumulation at this section, *i.e.* during glacial periods, would be most likely influenced by changes in dust source and the dust-transporting wind strength. Therefore, the hiatus between 30–17 ka falls well within the last glacial period and could be viewed as a result of strong wind erosion in competition with rapid accumulation at the proximal sites near the source. Instead, more loess accumulation during the last deglaciation (after 17 ka) could be explained as more preservation possibly due to weaker winds.

The sedimentation rate of the HS section is shown in **Fig. 6**. In view of the fact that feldspar ages are more reliable when the ages of samples are older than 50 ka, we calculated the sedimentation rates based on quartz ages during ~11 ka to ~8 ka, ~17–11 ka and ~34 ka to ~30 ka, and 75–34 ka on feldspar ages. The graph indicates two relatively rapid sedimentation rates during ~11 ka to ~8 ka with 32.0 ± 5.5 cm/ka, and ~34 ka to ~30 ka with 54.8 ± 1.1 cm/ka. Loess deposited at much slower accumulation rates of 5.5 ± 0.8 cm/ka and 5.0 ± 0.3 cm/ka during ~17–11 ka and ~75–34 ka, respectively. The loess sedimentation rate increases from 5.5 ± 0.8 cm/ka (17.1–10.9 ka) to 32.0 ± 5.5 cm/ka (10.9–8.5 ka) at 10.9 ± 0.6 ka (**Fig. 6**), which is close to the MIS 2/1 boundary. Higher sedimentation rate during the Holocene epoch (after about 11 ka), compared to the relatively low rate during the late glacial period, could be actually resulted from post-depositional disturbance (Lu *et al.*, 2006; Sun *et al.*, 2010; Xu *et al.*, 2018). The influence by post-depositional disturbance (*i.e.* bioturbation during pedogenesis) induced by more monsoon precipitation in the CSM region may be significant. It may homogenize sediments, disturb the underlying loess deposits and may offset the measured OSL age (Stevens *et al.*, 2007; Sun *et al.*, 2010; Xu *et al.*, 2018), the same sedimentary processes as the distal sites on the CLP behave (Xu *et al.*, 2018).

The rapid sedimentation rate during 34–30 ka was also similar with the lake sediments records (An *et al.*, 2012) suggested a rapid dust deposition during 32–29 ka and rapid loess sediments around 33–30 ka (Wang *et al.*, 2015). This similarity in loess sedimentation may have important implications for understanding the mechanism of loess accumulation and the process of palaeoclimatic changes. This still deserves further investigations.

5. CONCLUSIONS

We applied high-resolution luminescence dating, using both quartz OSL and K-feldspar $pIRIR_{290}$ on a loess sequence in the CSM, eastern China. The quartz signal is sensitive, fast component dominated, saturates approximately ~150 Gy. For K-feldspar $pIRIR_{290}$, first IR stimulation plateau tests indicated that the determined D_e does not have any obvious dependence on first IR stimulation temperature between 50°C and 260°C, and the dose recovery is satisfactory. In addition, K-feldspar $pIRIR_{290}$ signals are far from saturation and show an agreement with the expected stratigraphy (8~75 ka). Especially, the K-feldspar Post-IR IRSL dating method is the first application of the Loess dating in CSM region, implying that the experimental method has a large potential in the study of the older loess here.

Based on our results, a hiatus of ~13 ka between ~30 and ~17 ka can be interpreted as deflation, which indicates that it is an erosion area during 30–17 ka. This loess sequence provides a relatively long-term chronological basis of palaeoclimatic researches in this semi-humid region since the last glacial period.

ACKNOWLEDGEMENTS

We are grateful to two anonymous reviewers for their helpful comments and suggestions and prof. Liping Zhou for improving the English language of the final version. Thanks are extended to prof. Qingzhen Hao, Dr Shugang Kang, Dr Shuangwen Yi, Dr Yali Zhou and Fengyue Qiu for constructive discussions, to Yugeng Liu, Zhen Liu, Xiaoli Li, Xianan Hu and Tingwen Kou for their assistance in the field sampling. This work was supported by the National Nature Science Foundation of China (41602353, 41472313, 41402319 and 41877442).

REFERENCES

An ZS, Kutzbach JE, Prell WL and Porter SC, 2001. Evolution of Asian monsoons and phased uplift of the Himalaya–Tibetan plateau since Late Miocene times. *Nature* 411: 62–66, DOI 10.1038/35075035.

An ZS, Colman SM, Zhou WJ, Li XQ, Brown ET, Jull AJT, Cai YJ, Huang YS, Lu XF, Chang H, Song YG, Sun YB, Xu H, Liu WG, Jin ZD, Liu XD, Cheng P, Liu Y, Ai L, Li XZ, Liu XJ, Yan LB, Shi ZG, Wang XL, Wu F, Qiang XK, Dong ZB, Lu FY and Xu XW, 2012. Interplay between the Westerlies and Asian monsoon

recorded in Lake Qinghai sediments since 32 ka. *Scientific Reports* 2: 1–7, DOI 10.1038/srep 00619.

Ballarini M, Wallinga J, Wintle AG and Bos AJJ, 2007. A modified SAR protocol for optical dating of individual grains from young quartz samples. *Radiation Measurements* 42: 360–369, DOI 10.1016/j.radmeas.2006.12.016.

Bøtter-Jensen L, Thomsen KJ and Jain M, 2010. Review of optically stimulated luminescence (OSL) instrumental developments for retrospective dosimetry. *Radiation Measurements* 45: 253–257, DOI 10.1016/j.radmeas.2009.11.030.

Buylaert JP, Murray AS, Vandenberghe D, D_e Corte F and Vandenhaute P, 2008. Optical dating of Chinese loess using sand-sized quartz: establishing a time frame for late Pleistocene climate changes in the western part of the Chinese loess plateau. *Quaternary Geochronology* 3: 99–113, DOI 10.1016/j.quageo.2007.05.003.

Buylaert J-P, Murray AS, Thomsen KJ and Jain M, 2009. Testing the potential of an elevated temperature IRSL signal from K-feldspar. *Radiation Measurements* 44: 560–565, DOI 10.1016/j.radmeas.2009.02.007.

Buylaert J-P, Jain M, Murray AS, Thomsen KJ, Thiel C and Sohbati R, 2012. A robust feldspar luminescence dating method for Middle and Late Pleistocene sediments. *Boreas* 41: 435–451, DOI 10.1111/j.1502-3885.2012.00248.x.

Chapot MS, Roberts HM, Duller GAT and Lai ZP, 2012. A comparison of natural- and laboratory-generated dose response curves for quartz optically stimulated luminescence signals from Chinese Loess. *Radiation Measurements* 47: 1045–1052, DOI 10.1016/j.radmeas.2012.09.001.

Chen YW, Li SH, Li B, Hao QZ and Sun JM, 2015. Maximum age limitation in luminescence dating of Chinese loess using the multiple-aliquot MET-pIRIR signals from K-feldspar. *Quaternary Geochronology* 30: 207–212, DOI 10.1016/j.quageo.2015.01.002.

Cunningham AC and Wallinga J, 2010. Selection of integration time intervals for quartz OSL decay curves. *Quaternary Geochronology* 5: 657–666, DOI 10.1016/j.quageo.2010.08.004.

Ding ZL, Xiong SF, Sun JM, Yang SL, Gu ZY and Liu TS, 1999. Pedostratigraphy and paleomagnetism of a ~7.0 Ma eolian loess-red clay sequence at Lingtai, Loess Plateau, north-central China and the implications for palaeomonsoon evolution. *Palaeogeography, Palaeoclimatology, Palaeoecology* 152: 49–66, DOI 10.1016/S0031-0182(99)00034-6.

Duller GAT, 2003. Distinguishing quartz and feldspar in single grain luminescence measurements. *Radiation Measurements* 37: 161–165, DOI 10.1016/s1350-4487(02)00170-1.

E CY, Sohbati R, Murray AS, Buylaert JP, Liu XJ, Yang L, Yuan J and Yan WT, 2018. Hebei loess section in the Anyemaqen Mountains, northeast Tibetan Plateau: a high-resolution luminescence chronology. *Boreas* 47(4): 1170–1183, DOI 10.1111/bor.12321.

Fang XM, Li JJ and Van RVD, 1999. Rock magnetic and grain size evidence for intensified Asian atmospheric circulation since 800,000 years B.P. related to Tibetan uplift. *Earth and Planetary Science Letters* 165(1): 129–144, DOI 10.1016/s0012-821x(98)00259-3.

Fu X and Li SH, 2013. A modified multi-elevated-temperature post-IR IRSL protocol for dating Holocene sediments using K-feldspar. *Quaternary Geochronology* 17: 44–54, DOI 10.1016/j.quageo.2013.02.004.

Guo ZT, Rudiman WF, Hao QZ, Wu HB, Qiao YS, Zhu RX, Peng SZ, Wei JJ, Yuan B Y and Liu TS, 2002. Onset of Asian desertification by 22 Myr ago inferred from loess deposits in China. *Nature* 416: 159–163, DOI 10.1038/416159a.

Hansen V, Murray AS, Buylaert J-P, Yao E and Thomsen KJ, 2015. A new irradiated quartz for beta source calibration. *Radiation Measurements* 81: 123–127, DOI 10.1016/j.radmeas.2015.02.017.

Hao QZ, Wang L, Oldfield F, Peng SZ, Qin L, Song Y, Xu B, Qiao YS, Bloemendal J and Guo ZT, 2012. Delayed build-up of Arctic ice sheets during 400,000-year minima in insolation variability. *Nature* 490: 393–396, DOI 10.1038/nature11493.

Hao QZ, Guo ZT, Qiao YS, Xu B and Oldfield F, 2010. Geochemical evidence for the provenance of middle Pleistocene loess deposits in Southern China. *Quaternary Science Reviews* 29: 3317–3326, DOI 10.1016/j.quascirev.2010.08.004.

Huntley DJ and Baril MR, 1997. The K content of the K-feldspars being measured in optical dating or in thermoluminescence dating. *Ancient TL* 15: 11–13.

Jain M, Murray AS and Bøtter-Jensen L, 2003. Characterisation of blue-light stimulated luminescence components in different quartz samples: implications for dose measurement. *Radiation Measurements* 37 (4–5): 441–449, DOI 10.1016/s1350-4487(03)00052-0.

Jain M and Ankjærgaard C, 2011. Towards a non-fading signal in feldspar: insight into charge transport and tunneling from time resolved optically stimulated luminescence. *Radiation Measurements* 46: 292–309, DOI 10.1016/j.radmeas.2010.12.004.

Kong FB, Xu SJ and Jia GJ, 2017. Climatic and environmental evolution with multi-index records of the loess in the Focun, Zibo, Shandong Province. *Journal of Earth Environment* 8(5): 407–418 (In Chineses).

Lai ZP, Zhou J, Xia YF, Wang YJ and Chen J, 2001. Luminescence geochronology of Xiashu loess near Nanjing. *Journal of Desert Research* 21: 116–121 (In Chinese).

Lai ZP, 2010. Chronology and the upper dating limit for loess samples from Luochuan section in the Chinese Loess Plateau using quartz OSL SAR protocol. *Journal of Asian Earth Sciences* 37: 176–185, DOI 10.1016/j.jseaes.2009.08.003.

Li B and Li SH, 2011. Luminescence dating of K-feldspar from sediments: A protocol without anomalous fading correction. *Quaternary Geochronology* 6: 468–479, DOI 10.1016/j.quageo.2011.05.001.

Li B and Li SH, 2012. A reply to the comments by Thomsen *et al.* on 'Luminescence dating of K-feldspar from sediments : a protocol without anomalous fading correction'. *Quaternary Geochronology* 8: 49–51, DOI 10.1016/j.quageo.2011.10.001.

Li SH, Sun JM and Zhao H, 2002. Optical dating of dune sands in the northeastern deserts of China. Palaeogeography. Paleoclimatology. *Palaeoecology* 181: 419–429, DOI 10.1016/S0031-0182(01)00443-6.

Lisiecki LE and Raymo ME, 2005. A Pliocene-Pleistocene stack of 57 globally distributed benthic δ18O records. *Paleoceanography* 20: 1–17, DOI 10.1029/2004PA001071.

Liu LJ, Li PY and Wang YJ, 2000. The grain-size properties and genesis of the loess in central Shandong province. *Marine Geology & Quaternary Geology* 20(1): 81–86 (In Chinese).

Lu HY, Zhang FQ, Liu XD and Duce R, 2004. Periodicities of palaeoclimatic variations recorded by loess-paleosol sequence in China. *Quaternary Science Reviews* 23(18–19): 1891–1900, DOI 10.1016/j.quascirev.2004.06.005.

Lu HY, Stevens T, Yi SW and Sun XF, 2006. An erosional hiatus in Chinese loess sequences revealed by closely spaced optical dating. *Chinese Science Bulletin* 51: 2253–2259, DOI 10.1007/s11434-006-2097-x.

Mao MK, 1993. A study on regional structure of landforms in Shandong Province. *Scientla Geographica Sinica* 13(1): 26–33.

Mejdahl V, 1987. Internal radioactivity in quartz and feldspar grains. *Ancient TL* 5:10–17.

Murray AS and Wintle AG, 2003. The single aliquot regenerative dose protocol: potential for improvements in reliability. *Radiation Measurements* 37: 377–381, DOI 10.1016/s1350-4487(03)00053-2.

Murray AS and Wintle AG, 2000. Luminescence dating of quartz using an improved single-aliquot regenerative-dose protocol. *Radiation Measurements* 32: 57–73, DOI 10.1016/S1350-4487(99)00253-X.

Murray AS, Schmidt ED, Stevens T, Buylaert J-P, Marković SB, Tsukamoto S and Frechen M, 2014. Dating Middle Pleistocene loess from Stari Slankamen (Vojvodina. Serbia)—Limitations imposed by the saturation behaviour of an elevated temperature IRSL signal. *Catena* 117: 34–42, DOI 10.1016/j.catena.2013.06.029.

Peng SZ, Gao ZD, Wu XP, Zhang LB, Liang MY and Qiao YS, 2007. Grain-size distribution and genesis of loess in the Qingzhou area, Shandong. *Journal of Geomechanics* 13(4): 315–321(In Chinese).

Peng SZ, Hao QZ, Wang L, Ding M, Zhang W, Wang YN and Guo ZT, 2016. Geochemical and grain-size evidence for the provenance of loess deposits in the Central Shandong Mountains region, northern

China. *Quaternary Research* 85: 290–298, DOI 10.1016/j.yqres.2016.01.005.

Peng SZ, Zhu LJ, Xiao GQ, Qiao YS, Gao ZD and Chen DD, 2011. Magnetostratigraphy and provenance of the Qingzhou loess in Shandong Province. *Journal of Arid Land* 3 (3): 184–190, DOI 10.3724/SP.J.1227.2011.00184.

Prescott JR and Hutton JT, 1994. Cosmic ray contributions to dose rates for luminescence and ESR dating : large depths and long-term time variations. *Radiation Measurements* 23: 497–500, DOI 10.1016/1350-4487(94)90086-8.

Pye K, 1995. The nature, origin and accumulation of loess. *Quaternary Science Reviews* 14: 653–667, DOI 10.1016/0277-3791(95)00047-X.

Qiu FY and Zhou LP, 2015. A new luminescence chronology for the Mangshan loess-palaeosol sequence on the southern bank of the Yellow River in Henan, Central China. *Quaternary Geochronology* 30: 24–33, DOI 10.1016/j.quageo.2015.06.014.

Song YG, Fang XM, Torii M, Ishikawa N, Li JJ and An ZS, 2007. Late Neogene rock magnetic record of climatic variation from Chinese eolian sediments related to uplift of the Tibetan Plateau. *Jornal of Asian Earth Sciences* 30: 324–332, DOI 10.1016/j.jseaes.2006.10.004.

Stevens T, Thomas DSG, Armitage SJ, Lunn HR and Lu HY, 2007. Reinterpreting climate proxy records from late Quaternary Chinese loess: A detailed OSL investigation. *Earth-Science Reviews* 80: 111–136, DOI 10.1016/j.earscirev.2006.09.001.

Stevens T, Buylaert JP, Thiel C, Újvári G, Yi SW, Murray AS, Frechen M and Lu HY, 2018. Ice-volume-forced erosion of the Chinese Loess Plateau global Quaternary stratotype site. *Nature Communications* 9: 983, DOI 10.1038/s41467-018-03329-2.

Sun YB, Wang XL, Liu QS, and Clemens SC, 2010. Impacts of post-depositional processes on rapid monsoon signals recorded by the last glacial loess deposits of northern China. *Earth and Planetary Science Letters* 289: 171–179, DOI 10.1016/j.epsl.2009.10.038.

Thiel C, Buylaert J-P, Murray AS, Terhorst B, Hofer I, Tsukamoto S and Frechen M, 2011. Luminescence dating of the Stratzing loess profile (Austria) – Testing the potential of an elevated temperature post-IR IRSL protocol. *Quaternary International* 234: 23–31, DOI 10.1016/i.quaint.2010.05.018.

Thomsen KJ, Murray AS, Jain M and Bøtter-Jensen L, 2008. Laboratory fading rates of various luminescence signals from feldspar-rich sediment extracts. *Radiation Measurements* 43: 1474–1486, DOI 10.1016/j.radmeas.2008.06.002.

Wang XY, Yi SW, Lu HY, Vandenberhe J and Han ZY, 2015. Aeolian process and climatic changes in loess records from the northeastern Tibetan Plateau: response to global temperature forcing since 30 ka. *Paleoceanography* 30: 612–620, DOI 10.1002/2014pa00273.

Wang YX, Chen TY, E CY, An FY, Lai ZP, Zhao L and Liu XJ, 2018. Quartz OSL and K-feldspar post-IR IRSL dating of loess in the Huangshui river valley, northeastern Tibetan plateau. *Aeolian Reserch* 33: 23–32, DOI 10.1016/j.aeolia.2018.04.002.

Wintle AG, 1973. Anomalous fading of Thermo-luminescence in Mineral Samples. *Nature* 245: 143–144, DOI 10.1038/245143a0.

Wintle AG and Murray AS, 2006. A review of quartz optically stimulated luminescence characteristics and their relevance in single-aliquot regeneration dating protocols. *Radiation Measurements* 41: 369–391, DOI 10.1016/j.radmeas.2005.11.001.

Xu SJ, Ding XC, Yu LP and Ni ZC, 2015. Palaeoclimatic implications of aeolian sediments on the Miaodao Islands, Bohai Sea, East China, based on OSL dating and proxies. *Aeolian Research* 19: 259–266, DOI 10.1016/j.aeolia.2015.02.001.

Xu SJ, Kong FB, Jia GJ, Miao XD and Ding XC, 2017. An integrated OSL chronology, sedimentology and geochemical approach to loess deposits from Tuoji Island, Shandong Province: Implications for the late quaternary paleoenvironment in East China. *Aeolian Research* 31: 105–116, DOI 10.1016/j.aeolia.2017.07.007.

Xu SJ, Ding XC and Ni ZC, 2014. The sedimentary characteristics of Buxi loess profile in Shandong Province and their paleoclimatic and palaeoenvironmental significance. *Acta Geographica Sinica* 69(11): 1707–1717, DOI 10.11821/dlxb201411011.

Xu ZW, Stevens T, Yi SW, Mason J A and Lu HY, 2018. Seesaw pattern in dust accumulation on the Chinese Loess Plateau forced by late glacial shifts in the East Asian monsoon. *Geology* 46(10): 871–874, DOI 10.1130/G45105.1.

Yang SL, Forman LS, Song YG, Pierson J, Mazzocco J, Li XX, Shi ZT and Fang XM, 2014. Evaluating OSL-SAR protocols for dating quartz grains from the loess in Ili Basin, Central Asia. *Quaternary Geochronology* 20: 78–88, DOI 10.1016/j.quageo.2013.11.004.

Yi SW, Li XS, Han ZY, Lu HY, Liu JF and Wu J, 2017. High resolution luminescence chronology for Xiashu Loess deposits of Southeastern China. *Journal of Asian Earth Sciences* 155: 188–197, 10.1016/j.jseaes.2017.11.027

Yi SW, Buylaert J-P, Murray AS, Lu HY, Theil C and Zeng L, 2016. A detailed post-IR IRSL dating study of the Niuyanzigou loess site in northeastern China. *Boreas* 45: 644–657, DOI 10.1111/bor.12185.

Yi SW, Buylaert J-P, Murray AS, Thiel C, Zeng L and Lu HY, 2015. High resolution OSL and post-IR IRSL dating of the last interglacial-glacial cycle at the Sanbahuo loess site (northeastern China). *Quaternary Geochronology* 30: 200–206, DOI 10.1016/j.quageo.2015.02.013.

Zhang ZL, Xin LJ and Nie XH, 2004. A summary of Loessial Researches in Shandong. *Scientia Geographica Sinica* 24(6): 746–752 (In Chinese).

Zhang ZL, Xin LJ, Jiang LG and Huang P, 2005. Sedimentary characteristics and genetic analysis of Zhangxia Loess in Jinan, Shandong Province. *Journal of Palaeogeography* 7: 98–106, DOI 10.1360/gs050303.

Zheng HH, Zhu ZY, Huang BL, Lu LC, 1994. A study on loess geochronology of Shandong peninsula and northern part of Jiangsu and Anhui provinces. *Marine Geology and Quaternary Geology* 14(1): 63–68 (In Chinese).